Artificial localized magnon resonances in subwavelength meta-particles

Cite as: Appl. Phys. Lett. **113**, 123505 (2018); https://doi.org/10.1063/1.5047445
Submitted: 06 July 2018 . Accepted: 08 September 2018 . Published Online: 21 September 2018

Dmitry Filonov, Andrey Shmidt, Amir Boag, and Pavel Ginzburg

Artificial localized magnon resonances in subwavelength meta-particles

Dmitry Filonov,[1,a)] Andrey Shmidt,[1] Amir Boag,[1] and Pavel Ginzburg[1,2]
[1]School of Electrical Engineering, Tel Aviv University, Tel Aviv 69978, Israel
[2]Light-Matter Interaction Centre, Tel Aviv University, Tel Aviv 69978, Israel

(Received 6 July 2018; accepted 8 September 2018; published online 21 September 2018)

The interaction between electromagnetic waves and objects is strongly affected by the shape and material composition of the latter. Artificially created materials, formed by a subwavelength structuring of their unit cells, namely metamaterials, can exhibit peculiar responses to electromagnetic radiation and provide additional powerful degrees of freedom to the scatterer design. In particular, negative material susceptibilities give rise to strong resonant interactions with deeply subwavelength particles. While the negative electrical permittivity of natural noble metals manifests itself in localized plasmon resonant oscillations, negative magnetic permeability materials are rare in nature. Here, the concept of artificial magnon resonance in subwavelength objects with effective negative permeability, designed via the metamaterial approach, is demonstrated. Strong localized oscillations of the magnetic fields within an array of split ring resonators, forming a sphere, hybridize in a collective mode of the structure. As a result, a high scattering cross section, exceeding that of a steel sphere with the same radius by four orders of magnitude, was demonstrated. Scatterers, based on tunable resonances within artificially created materials, can find use in a broad range of electromagnetic applications, including wireless communications, radars, RFID, internet of things hardware, and many others. *Published by AIP Publishing.* https://doi.org/10.1063/1.5047445

Interactions of electromagnetic waves with material structures give rise to many fundamental phenomena, occurring over the whole spectral range [e.g., optical[1] and low MHz–GHz (Ref. 2)] and drive to a vast variety of modern applications. Scattering cross sections (SCSs) of objects are solely defined by their geometries and material compositions. A span of optical materials is rather broad, which allows considering the material degree of freedom as a design parameter. For example, noble metals, such as silver and gold, have moderate negative permittivity in visible and infrared spectral ranges. This property enables observing and controlling resonant scattering phenomena from deeply subwavelength geometries and it is referred to as localized plasmon resonance (LPR), e.g., see Refs. 3 and 4. However, metals exhibit extreme negative epsilon behavior and become primarily conductive in low-frequency ranges, virtually eliminating the ability to support the LPR phenomenon. Consequently, achieving resonant behavior of structures in MHz–GHz frequency ranges requires the utilization of retardation effects, which imposes limitations on linear dimensions of scatterers.[2] Reducing the physical sizes of antennas, employed in wireless communication links, is a long-standing task which requires exploring tradeoffs between many parameters, pre-defining the performance. However, material properties, in the majority of the cases, are rarely considered as valuable degrees of freedom, which can bring qualitatively new concepts into the field. High epsilon ceramic composites[5] are worth mentioning, as they enable shrinking effective wavelengths by orders of magnitude. Also, magnetically biased ferrite-based materials can exhibit both high positive and negative nonreciprocal permeabilities in the GHz spectral range.[6,7] These materials, however, require complex fabrication routines and hardly sustain post processing due to their brittle nature. One of the very promising concepts for tailoring material properties, which was found to be successful in applications in the MHz–THz frequency ranges, is developing arrays and surfaces with subwavelength structuring. Properties of those artificially created composites can be homogenized and encapsulated within effective permittivity and permeability parameters—this is the concept of metamaterials.[8–12] Radio frequency (RF) metamaterials were suggested and demonstrated for invisibility cloaking,[13] scattering suppression,[14] negative refraction,[15] super-resolution imaging,[16] metamaterial-based cavities,[17] compact cavity resonators,[18] emulation tools for complex optical phenomena (e.g., Ref. 19) antennas with improved characteristics, (e.g., Refs. 20–22) and many others. Recently, extremely subwavelength metamaterials for MHz applications have been demonstrated, e.g., Refs. 23 and 24. Negative permittivity and permeability (in separate) composites are especially relevant to the current investigation. For example, a wire medium was proposed to serve as an artificial plasmonic material ($\varepsilon < 0$) at RF,[25] while strong spatial dispersion should be taken into account in order to extract effective material parameters.[26] Other types (resonant) of artificial RF plasmonic materials were demonstrated in an application to the invisibility cloaking.[27] Several proposals and analytical investigations on electrically small antennas with negative effective parameters were reported, e.g., Refs. 28 and 29.

While realizations of strong collective electric responses require the employment of dipolar-like resonators within an array, magnetic phenomena are governed by microscopic (on the subwavelength scale in the context of metamaterials) circular currents. Split ring resonators (SRRs) are frequently employed for achieving artificial magnetic responses, e.g., see Refs. 30 and 31. Limitations of the homogenization

a)dimfilonov@gmail.com

theory in application to the analysis of finite size SRR-based geometries were recently analyzed and relatively small deviations were shown to emerge owing to modifications in boundary conditions.[32] If the collective response of near-field coupled SRRs (or other types of resonators) is strong enough, the homogenized effective permeability can become negative. As a result, small subwavelength structures can exhibit strong localized resonances, driven by magnetic fields, in a similarity to LPR. This effect will be investigated hereafter and taken towards applications, where high Scattering Cross Sections (SCSs) are required.

The manuscript is organized as follows: the effect of an artificial localized magnon resonance will be introduced and homogenization procedures towards achieving negative effective permeability in SRR arrays will be introduced at first. A design of a deeply subwavelength metamaterial-based sphere, operating in the MHz frequency range, will follow. It will be shown that a small metamaterial-based object, as small as 10 cm in diameter, can have a VHF radar signature, comparable with those of big aircrafts. The design, full numerical analysis, and experimental study in the GHz spectral range will come before the conclusions.

The LPR phenomenon utilizes collective oscillations of conduction electrons within noble metals and causes small deeply subwavelength particles to exhibit strong resonant responses. For example, the 5 nm gold sphere resonates at 500 nm, demonstrating performance of an efficient electromagnetically small resonator, which is as small as $\lambda/100$ in size.[3] Relying on the duality of electric and magnetic fields, intrinsic to Maxwell's equations, a similar phenomenon is expected to emerge in the case of negative permeability structures. In this case, the polarizability of a small magnetic sphere is given by

$$\alpha_m = 4\pi r^3 \left(\frac{\mu_r - 1}{\mu_r + 2}\right), \tag{1}$$

where μ_r is the relative permeability of the material, while r is the radius of the sphere. This expression can be modified to include the retardation effects, if the skin depth (for magnetic field penetration) becomes comparable with the radius. With the full analogy to the electric particles,[33,34] the modified polarizability is given by

$$\alpha_m = 4\pi \left(\frac{1}{r^3} \times \frac{\mu_r + 2}{\mu_r - 1} - i\frac{2}{3}k^3 - \frac{k^2}{r}\right)^{-1}, \tag{2}$$

where k is the free space wavenumber of the incident radiation. Eq. (1) explicitly shows that the resonant conditions are obtained when $Re(\mu_r) = -2$ and the quality factor of the resonance is limited by the material and radiation (Eq. 2) losses. Following the terminology of the localized plasmon resonance in the case of $Re(\varepsilon_r) = -2$, the magnetic phenomenon was coined here by the name of localized magnon resonances with the classification "artificial" in order not to confuse it with the true solid state effect of collective excitation of the electrons' spins in a crystal lattice.[35]

It is worth noting that the resonant condition of Eq. (1) strongly depends on the geometry and can be tuned by its adjustment, e.g., see Refs. 4 and 36. Spherical geometry will be chosen hereafter only for the sake of the analytical simplicity of the analysis.

In contrast to negative permittivity, negative permeability materials are very rare in nature. Nevertheless, they can be created artificially by constructing arrays of ring resonators, which mimic a crystal of microscopic magnetic spins. The additional gap with or without a lumped capacitor element can be added within the ring in order to tune the resonance of the structure to a desired frequency.[31] The layout and parameters of the split ring resonator appear in the inset in Fig. 1(a). Identical SRRs were placed at the nodes of a 3D array (at the nodes of a simple cubic crystal with the period a) and effective electric and magnetic susceptibilities were retrieved. While an ideal array of rings can be homogenized analytically by applying coupled dipole summations,[37] a full wave numerical simulation with CST Microwave Studio was performed here (frequency domain solver with 10^{-9} convergence parameter for very accurate modeling). It allows taking into account the effects of asymmetry, impact of substrates and losses, and higher order electric and magnetic couplings, which are ignored in the beforehand mentioned analytical approach. A typical two-port waveguide system, with relevant dimensions to the specific frequency range, was used. Complex-valued transmission and reflection coefficients (S-parameters) were calculated for three different orientations, corresponding to the main crystallographic axis

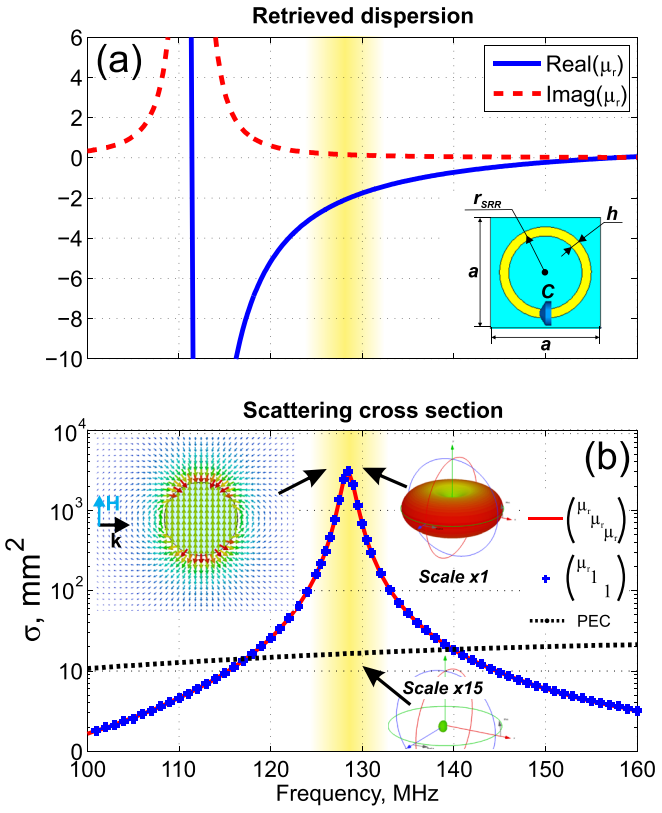

FIG. 1. (a) Dispersion of the homogenised array of split ring resonators (in the inset). Blue line—real part of the relative permeability, red dashed line—its imaginary part. Parameters of the array appear in the text. (b) Scattering cross section spectra of a 5 cm radius sphere made of a homogeneous material: red line—isotropic, blue dots—anisotropic, black dots—made of a perfect electric conductor. Insets—(top-right) scattering patterns of the structures [meta-sphere in 1:1 scale, (bottom-right) PEC sphere in 1:15 scale for a better visibility], (left) - magnetic field distribution of the resonant magnetic dipole mode.

of the metamaterial, and the permittivity and permeability tensors were extracted, following the formulation, reported in Ref. 38. The following parameters of the structure were chosen after a set of optimizations: $r_{SRR} = 2.5$ mm, $h = 0.5$ mm, $a = 6$ mm, and $C = 220$ pF. The substrate was taken to be *Isola IS680 AG338* ($\varepsilon = 3.38$, $tg\delta = 0.0026$) of 1.5 mm thickness, and the material of the SRR is copper (conductivity of 5.96×10^7 S/m). The resulting dispersion of effective magnetic medium appears in Fig. 1(a). Both real and imaginary parts resemble the classical Lorentzian shape close to the collective resonance. The region of interest, where the effective real part of the permeability approaches the value of **−2,** is highlighted with the yellow shadow. Effective permeability is calculated and this frequency range is ∼2.4 (Note that electric and magnetic phenomena are virtually decoupled in deeply subwavelength particles and the electric contribution of the particle to the SCS is minor). The corresponding frequency was chosen to fall within the region of VHF radar operation[39] for a demonstration of the concept only. It is worth emphasizing that the homogenised arrays of planar rings have strongly anisotropic permeability tensor—Fig. 1(a) demonstrates its component along the normal to the rings, while other two are virtually equal to unity. As a result, the composite behaves as a hyperbolic metamaterial[40] for the magnetic field. "Hyperbolic" effects, however, do not play a role here and are mentioned only owing to the special form of the effective tensor.

The scattering cross-section spectrum of the 5 cm sphere, made of the artificial magnetic material, appears in Fig. 1(b). Two scenarios for the material permeability were considered here—isotropic μ_r and hyperbolic tensor, discussed beforehand. In deep subwavelength geometries, where the scattered field is known to be uniform inside the sphere, both of the cases demonstrate exactly the same behavior (polarization of the incident magnetic field is assumed to be along the direction of the nontrivial tensor component). The comparison between the meta-scatterer and a solid sphere, made of a perfect electric conductor (PEC), appears in Fig. 1(b). Four orders of magnitude in the SCS enhancement owing to the artificial localized magnon resonance can be observed. Insets to panel b demonstrate the comparison of scattering diagrams on the linear scale. Note that data for the PEC sphere are multiplied by a factor of 15 in order to make it visible. This significant enhancement makes the SCS of the sphere to comparable to the VHF radar signature of a big aircraft.[41] Note that both objects are subwavelength in the case of VHF radar applications. The advantage of the localized magnon resonance in scattering applications over high-quality resonators, made of high permittivity ceramic materials, is also worth mentioning. For example, 5 cm radius spheres, made of $BaTiO_3$-$SrTiO_3$ with $\varepsilon = 533$ and $tg\delta = 0.018$,[42] have a dipolar resonance at 130 MHz. The SCS peak of this structure is 30 times smaller than the value, demonstrated by the metamaterial-based scatterer, underlining the strength of the proposed approach. Furthermore, the metamaterial structure scatters 12 times more than all the constitutive SRRs, if they were uncoupled.

To verify the magnetic nature of the resonance, the far- and near-field patterns of the scattered fields were calculated. Figure 2 demonstrates the comparison between the fields,

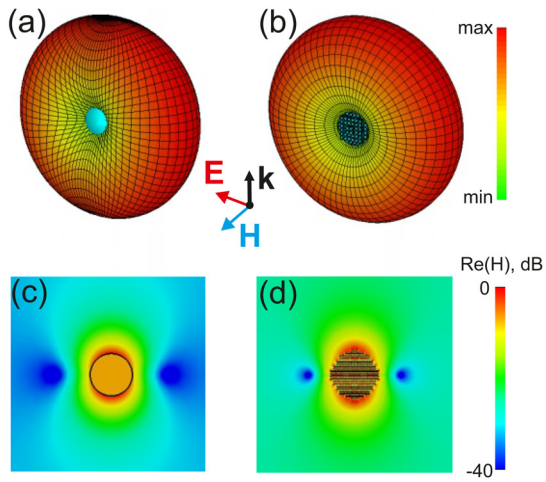

FIG. 2. Comparison between the homogeneous sphere [Lorentz dispersion, Fig. 1(a)] [panels (a) and (c)] and the SRR-based metamaterial structure [panels (b) and (d)]. Scattered far-field pattern (H-field intensity)—panels (a) and (b). Near-field distribution Real part (H-field)—panels (c) and (d).

obtained for the sphere, made of a homogenized material [Lorentz dispersion from Fig. 1(a)] [panels (a) and (c)] and the full wave simulation of the entire structure, consisting of 420 elements [panels (b) and (d)]. Both near- and far-field distributions agree extremely well with each other, supporting the claim of the magnetic nature of the resonance inside the metamaterial-based sphere.

In order to demonstrate the beforehand discussed phenomena, experimental studies will be performed in the GHz spectral range. The choice of the frequency band is solely pre-defined by the available experimental facilities (anechoic chamber). The same retrieval procedure was employed in order to extract and optimize effective parameters of SRR arrays. In fact, exactly the same geometric parameters, as in the beforehand MHz case, were used apart from the lumped capacitor, which was taken here to be $C = 0.5$ pF. Effective permeability dispersion appears in Fig. 3(a). In contrary to the MHz realization, deep subwavelength structuring in the GHz spectral range requires accurate miniaturizing of resonators and soldering of lumped elements, which also start influencing the scattering owing to their packaging sizes. As a result, the fabrication aspects set additional constraints on the dimensions of the subwavelength structure, which start experiencing retardation effects. The color map in Fig. 3(b) shows the evolution of the SCS spectrum as a function of the sphere size. The spectra were obtained numerically, while the particle effective tensor was taken to be anisotropic (hyperbolic dispersion). The white line, showing the main SCS peak, was calculated with Eq. (2). While this analytical formula was derived for the purely isotropic case, it fits extremely well with the numerical data and shows the red-shift of the peak with the radius increase. This effect will be clearly observed in the forthcoming experimental results.

The experimental sample, following the effective medium design, was fabricated to maintain the same geometric parameters. The meta-sphere contains 13 layers, separated by a 5 mm distance (the period of the structure). SRR arrays were fabricated on low loss *Isola* pc-board (parameters appear in the previous paragraph) with standard

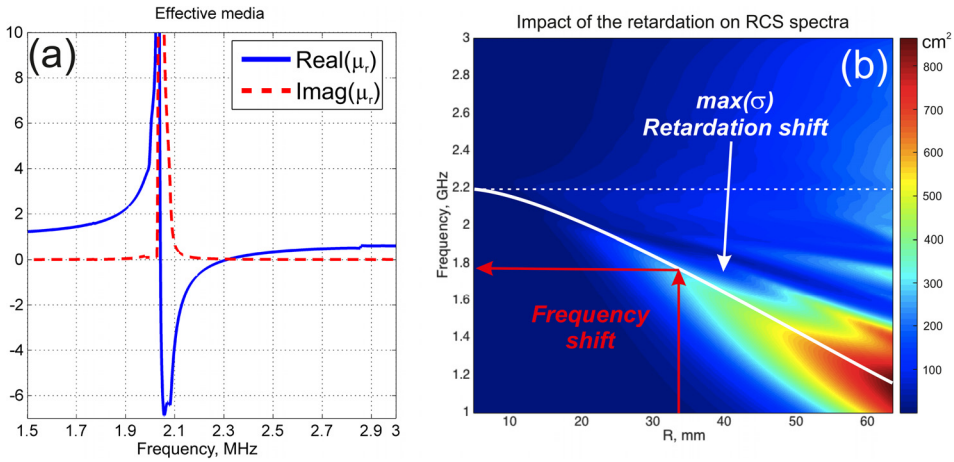

FIG. 3. (a) Retrieved relative permeability spectrum. Red dashed line—imaginary part, blue solid line—a real part of μ_{r_eff}. (b) Color map of the SCS spectra (frequency is along the vertical axis) as a function of the sphere radius (horizontal axis). The sphere is made of a material with homogeneous anisotropic permeability with the dispersion of the nontrivial component, which appears on the panel (a). The white dashed line represents the position of the SCS peak without considering the retardation effect [Eq. (1)]. The white solid line is calculated according to Eq. (2) and follows the SCS peak, underlining the influence of the retardation shift.

lithography, followed by chemical etching. Lumped elements (Multilayer Ceramic Capacitors 500R07S0R5AV4T) with a declared small tolerance (0.5%) in the nominal capacitance were soldered to the SRRs' gaps (542 elements in overall). The photograph of the sample appears in Fig. 4(c) (inset). A rectangular wideband horn (IDPH2018) antenna connected to the transmitting port of a Vector Network Analyzer (VNA E8362B) was used as a plane wave excitation source. The scatterer was then located in the far-field of the antenna (~2.5 m distance apart) and a second identical horn was used as a receiver to collect the signal. Absolute SCS values were obtained with a set of standard calibrations, including measurements, performed on a test metal sphere.[43]

Figure 4 shows the comparison between the prediction of the super scatterer's SCS and its actual measured performance. Panel (a) demonstrates the numerically obtained SCS spectrum of the homogenized sphere with the anisotropic magnetic tensor. The full wave simulation of the entire structure, including all 13 planes, containing 542 SRRs with lumped capacitors, was performed and the resulting SCS appears in Fig. 4(b). The lumped capacitors were incorporated in series into the second 0.4 mm gap in of the SRRs as real passive elements. Impedance characteristics and their tolerance were adopted from the vendor's datasheets. The experimental data are presented in panel (c). The excellent agreement between all three methods is worth noting. The main peak on the SCS spectrum corresponds to the dipolar resonance, which is calculated with Eq. (2) (recall the shift, originating from the retardation effect). The secondary peak, blue-shifted with respect to the main one, corresponds to the quadrupole mode. Its resonant condition is $Re(\mu_r) = -1.5$ in the fully quasistatic approximation. Its spectral location agrees with the dispersion curve of the effective medium [Fig. 3(a)]. The maximum SCS value is as high as 250 cm^2, which is almost one order of magnitude larger than the geometric area of the scatterer (πr^2). This ratio can be further increased, if SRRs will be replaced with higher quality factor resonators, the substrate losses and nominal dispersion of lumped elements will be improved.

In summary, the effect of artificial localized magnon resonance in arrays of near-field coupled split rings was demonstrated. Negative effective permeability was shown to be responsible for the high scattering cross-section of the metamaterial-based sphere. In particular, 5 cm radius (~1/50 fraction of a wavelength) scatterer can have a VHF radar signature, comparable with that of a big aircraft. Experimental demonstration of the concept at the GHz frequency band was found to be in extremely good agreement with theoretical predictions and full-wave numerical simulations. Scattering cross sections of the designed objects, operating at the localized magnon resonance, were found to prevail in the signatures of steel spheres and high-quality factor ceramic resonators by orders of magnitude. It is worth mentioning that there are no fundamental upper limitations on the SCS of a lossless object, if all scattering channels (multipoles) resonate at the same frequency.[44,45] The fundamental limit of one channel is $3\lambda^2/(2\pi)$. However, practical realizations of resonators, based on natural lossy materials and fabrication imperfections, are the limiting factors. The focus of this report was made on designing a single magnetic dipolar resonance. It is also worth motioning that the Chu–Harrington criterion (e.g., Ref. 46) sets the lower limit on quality factor

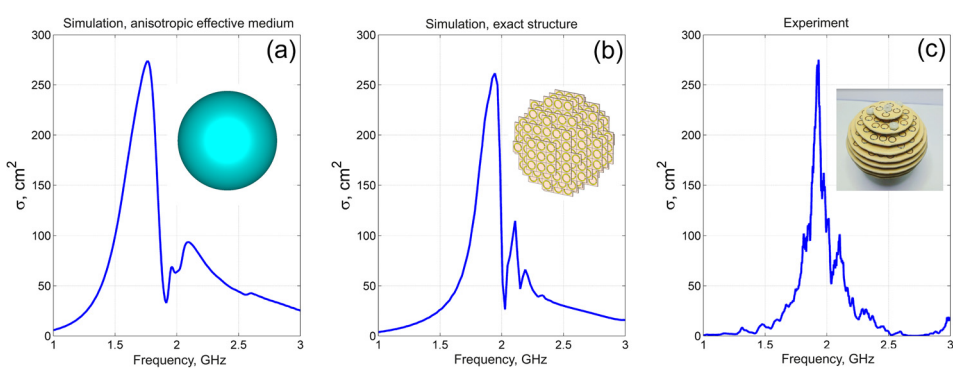

FIG. 4. Scattering cross section spectra of the metamaterial-based sphere with 33 mm radius. (a) Numerical modeling of the homogeneous anisotropic sphere. (b) Full wave numerical modeling of the metamaterial scatterer, made of split ring resonator arrays (13 planes, 542 SRRs in overall). (c) Experimental data for the sample, which follows the design of panel (b). Additional details appear in the main text.

of electrically small antennas, and it is not a restricting factor of SCS values.

The demonstrated concept of efficient magnetic scatterers paves the way for further development of many applications, including short and long-range wireless communications, efficient remote RFID tags and their use in internet of things protocols, and many other areas.

This work was partly supported by the PAZY foundation, Binational Science Foundation (project 2016059), and the Kamin Project.

[1]M. Born and E. Wolf, *Principles of Optics: Electromagnetic Theory of Propagation, Interference and Diffraction of Light*, 7th ed. (Cambridge University Press, 1999).
[2]C. E. Balanis, in *Antenna Theory: Analysis and Design*, 3rd ed., edited by C. A. Balanis (John Wiley & Sons, Inc., 2005), p. 1136.
[3]L. Novotny and B. Hecht, *Principles of Nano-Optics*, 2nd ed. (Cambridge University Press, 2012).
[4]N. Berkovitch, P. Ginzburg, and M. Orenstein, J. Phys. Condens. Matter **24**, 73202 (2012).
[5]C. A. Balanis, *Antenna Theory: Analysis and Design*, 3rd ed. (Wiley-Interscience, 2015).
[6]A. G. Gurevich and G. A. Melkov, *Magnetization Oscillations and Waves* (CRC Press, 1996).
[7]C. A. Balanis, *Advanced Engineering Electromagnetics* (Wiley, 1989).
[8]N. Engheta and R. W. Ziolkowski, *Metamaterials: Physics and Engineering Explorations*, 1 ed. (Wiley-IEEE Press, 2006).
[9]S. Tretyakov, A. Urbas, and N. Zheludev, J. Opt. **19**, 80404 (2017).
[10]W. Cai and V. Shalaev, *Optical Metamaterials* (Springer, New York, NY, 2010).
[11]S. B. Glybovski, S. A. Tretyakov, P. A. Belov, Y. S. Kivshar, and C. R. Simovski, Phys. Rep. **634**, 1 (2016).
[12]N. I. Zheludev and Y. S. Kivshar, Nat. Mater. **11**, 917 (2012).
[13]D. Schurig, J. J. Mock, B. J. Justice, S. A. Cummer, J. B. Pendry, A. F. Starr, and D. R. Smith, Science **314**, 977 (2006).
[14]D. S. Filonov, A. S. Shalin, I. Iorsh, P. A. Belov, and P. Ginzburg, J. Opt. Soc. Am. A **33**, 1910 (2016).
[15]R. A. Shelby, D. R. Smith, and S. Schultz, Science **292**, 77 (2001).
[16]F. Mesa, M. Freire, R. Marqués, and J. Baena, Phys. Rev. B **72**, 235117 (2005).
[17]H. Caglayan, I. Bulu, M. Loncar, and E. Ozbay, Opt. Express **16**, 11132 (2008).
[18]M. Caiazzo, S. Maci, and N. Engheta, IEEE Antennas Wireless Propag. Lett. **3**, 261 (2004).
[19]D. Filonov, Y. Kramer, V. Kozlov, B. A. Malomed, and P. Ginzburg, Appl. Phys. Lett. **109**, 111904 (2016).
[20]L.-W. Li, Y.-N. Li, T. S. Yeo, J. R. Mosig, and O. J. F. Martin, Appl. Phys. Lett. **96**, 164101 (2010).
[21]E. Lier, D. H. Werner, C. P. Scarborough, Q. Wu, and J. A. Bossard, Nat. Mater. **10**, 216 (2011).
[22]D. Yuandan and T. Itoh, Proc. IEEE **100**, 2271 (2012).
[23]W.-C. Chen, C. M. Bingham, K. M. Mak, N. W. Caira, and W. J. Padilla, Phys. Rev. B **85**, 201104 (2012).
[24]X. Zhang, E. Usi, S. K. Khan, M. Sadatgol, and D. O. Gueney, Prog. Electromagn. Res. **152**, 95 (2015).
[25]J. Pendry, A. Holden, W. Stewart, and I. Youngs, Phys. Rev. Lett. **76**, 4773 (1996).
[26]P. A. Belov, R. Marqués, S. I. Maslovski, I. S. Nefedov, M. Silveirinha, C. R. Simovski, and S. A. Tretyakov, Phys. Rev. B **67**, 113103 (2003).
[27]B. Edwards, A. Alù, M. G. Silveirinha, and N. Engheta, Phys. Rev. Lett. **103**, 153901 (2009).
[28]H. R. Stuart and A. Pidwerbetsky, IEEE Trans. Antennas Propag. **54**, 1644 (2006).
[29]C. Pfeiffer and A. Grbic, IEEE Trans. Antennas Propag. **60**, 1671 (2012).
[30]J. B. Pendry, A. J. Holden, D. J. Robbins, and W. J. Stewart, IEEE Trans. Microwave Theory Tech. **47**, 2075 (1999).
[31]F. Capolino, *Applications of Metamaterials* (CRC Press, 2009).
[32]M. Gorkunov, M. Lapine, E. Shamonina, and K. H. Ringhofer, Eur. Phys. J. B **28**, 263 (2002).
[33]B. T. Draine, Astrophys. J. **333**, 848 (1988).
[34]M. Meier and A. Wokaun, Opt. Lett. **8**, 581 (1983).
[35]F. Bloch, Z. Phys. **61**, 206 (1930).
[36]N. Berkovitch, P. Ginzburg, and M. Orenstein, Nano Lett. **10**, 1405 (2010).
[37]M. Lapine, A. K. Krylova, P. A. Belov, C. G. Poulton, R. C. McPhedran, and Y. S. Kivshar, Phys. Rev. B **87**, 24408 (2013).
[38]X. Chen, T. M. Grzegorczyk, B.-I. Wu, J. Pacheco, and J. A. Kong, Phys. Rev. E **70**, 16608 (2004).
[39]N. Levanon and E. Mozeson, *Radar Signals*, 1 ed. (Wiley-IEEE Press, 2004).
[40]H. N. S. Krishnamoorthy, Z. Jacob, E. Narimanov, I. Kretzschmar, and V. M. Menon, Science **336**, 205 (2012).
[41]J. G. Yuricich, *Applying Radar Cross-Section Estimations to Minimize Radar Echo in Unmanned Combat Air Vehicle Design* (The Ohio State University, 2016).
[42]See http://www.ceramics.sp.ru for material parameters of high quality ceramic elements.
[43]C. A. Balanis, *Antenna Theory: Analysis and Design*, 3 ed. (Wiley-Interscience, 2005).
[44]Z. Ruan and S. Fan, Phys. Rev. Lett. **105**, 13901 (2010).
[45]Z. Ruan and S. Fan, Appl. Phys. Lett. **98**, 43101 (2011).
[46]L. J. Chu, J. Appl. Phys. **19**, 1163 (1948).